Semi-analytical formulation for vibroacoustic response of a heavy fluid-loaded plate with ABH stiffeners

Daniel Martins, Mahmoud Karimi, Laurent Maxit

Thin-Walled Structures

Semi-analytical formulation for vibroacoustic response of a heavy fluid-loaded plate with ABH stiffeners

--Manuscript Draft--

Manuscript Number:	TWST-D-24-02245
Article Type:	Research Paper
Section/Category:	Analytical formulations
Keywords:	Bloch-Floquet waves, Acoustic black holes, Stiffened plate, Heavy fluid-loading
Corresponding Author:	Daniel Martins University of Technology Sydney AUSTRALIA
First Author:	Daniel Martins
Order of Authors:	Daniel Martins
	Mahmoud Karimi
	Laurent Maxit
Manuscript Region of Origin:	Asia Pacific
Abstract:	Stiffened structures are widely used in aeronautics, marine and rail industries. When stiffeners are integrated into host structures, so-called Bloch-Floquet waves are generated due to interactions between the host's flexural waves and the stiffeners' flexural and torsional waves. It is reported in the literature that these waves are often the source of undesirable noise and vibrations when the stiffened structure is excited by a force. To mitigate unwanted noise and vibrations from the stiffened structures, this study proposes to replace common rectangular stiffeners with Acoustic Black Hole (ABH) stiffeners. To do this, a semi-analytical model is initially developed in the wavenumber domain to predict the forced vibroacoustic response of a 2D fluid-loaded infinite plate with stiffeners on one side. In the proposed model, the stiffeners are characterized by their translational and rotational dynamic stiffnesses which can be estimated by a finite element method (FEM). These dynamic stiffnesses are then coupled with the analytical formulation of the fluid-loaded plate to obtain the expressions of the spectral displacement and radiated pressure. Comparisons of the results in terms of the plate's mean quadratic velocity and radiated sound power for the rectangular and ABH stiffeners show that by using the ABH stiffeners instead of the conventional stiffeners, one can significantly reduce the vibroacoustic response of the fluid-loaded plates.
Suggested Reviewers:	Brian Mace b.mace@auckland.ac.nz Honorary Academic and Emeritus Professor at University of Auckland, expert in stiffened structures.
	Jordan Cheer J.Cheer@soton.ac.uk Professor at University of Southampton, Chair in Smart Acoustic Control Technologies, and expert in acoustic black holes.
	Mikhail Mironov mironov_ma@mail.ru Principal Investigator at Andreyev Acoustics Institute, one of the pioneers of the acoustic black holes concept.
Opposed Reviewers:	

UTS
UNIVERSITY OF TECHNOLOGY, SYDNEY

3 June, 2024

Editorial Office

Thin-Walled Structures

Please find attached our manuscript entitled:

Semi-analytical formulation for vibroacoustic response of a heavy fluid-loaded plate with ABH stiffeners

by authors Daniel Martins, Mahmoud Karimi and Laurent Maxit for possible publication in Thin-Walled Structures.

Yours sincerely,

Daniel Martins

Centre for Audio, Acoustics & Vibration

School of Mechanical and Mechatronic Engineering

University of Technology, Sydney

Email: daniel.martins@students.uts.edu.au
SYDNEY, NSW - AUSTRALIA

Highlights

- A semi-analytical vibroacoustic model of fluid-loaded stiffened plates is developed.
- It is computationally efficient and can be used for plates with complex stiffeners.
- Vibroacoustic behaviour of heavy fluid-loaded plates with ABH stiffeners is studied.
- It is shown ABH stiffeners can significantly mitigate the vibroacoustic response.

Semi-analytical formulation for vibroacoustic response of a heavy fluid-loaded plate with ABH stiffeners

Daniel Martins[a], Mahmoud Karimi[a], Laurent Maxit[b]

[a]*Centre for Audio, Acoustics and Vibration, University of Technology Sydney, Sydney, Australia*
[b]*INSA Lyon, LVA, UR677, 25 bis av. Jean Capelle, 69621 Villeurbanne Cedex, France*

Abstract

Stiffened structures are widely used in aeronautics, marine and rail industries. When stiffeners are integrated into host structures, so-called Bloch-Floquet waves are generated due to interactions between the host's flexural waves and the stiffeners' flexural and torsional waves. It is reported in the literature that these waves are often the source of undesirable noise and vibrations when the stiffened structure is excited by a force. To mitigate unwanted noise and vibrations from the stiffened structures, this study proposes to replace common rectangular stiffeners with Acoustic Black Hole (ABH) stiffeners. To do this, a semi-analytical model is initially developed in the wavenumber domain to predict the forced vibroacoustic response of a 2D fluid-loaded infinite plate with stiffeners on one side. In the proposed model, the stiffeners are characterized by their translational and rotational dynamic stiffnesses which can be estimated by a finite element method (FEM). These dynamic stiffnesses are then coupled with the analytical formulation of the fluid-loaded plate to obtain the expressions of the spectral displacement and radiated pressure. Comparisons of the results in terms of the plate's mean quadratic velocity and radiated sound power for the rectangular and ABH stiffeners show that by using the ABH stiffeners instead of the conventional stiffeners, one can significantly reduce the vibroacoustic response of the fluid-loaded plates.

Keywords: Bloch-Floquet waves, Acoustic black holes, Stiffened plate, Heavy fluid-loading

1. Introduction

Predicting the forced vibroacoustic responses of stiffened structures is essential for designing various engineering applications, including aircraft fuselages and marine vessels. It is known that with the introduction of periodically spaced stiffeners into the structure, Bloch-Floquet (BF) waves are generated due to the interaction of the flexural waves of the host structure (plate, cylinder) with the flexural/torsional waves of the stiffeners [1, 2]. If these stiffeners are periodically spaced, the wave interaction will produce predictable passbands associated with higher vibration levels [2, 3]. Additionally, for certain frequencies within a passband, the BF waves will radiate significantly in the far-field when the BF wavenumbers are smaller than the acoustic wavenumber, resulting in undesirable noise in the far-field [4]. In this paper, we propose to use acoustic black holes (ABHs) to mitigate the contribution of the BF waves in the vibroacoustic response of a stiffened structure. This is achieved by replacing conventional rectangular stiffeners with ABH-shaped stiffeners.

ABHs have emerged as a notable strategy for mitigating vibrations in structures. An ideal ABH is an engineered structure featuring a continuously varying cross-sectional area that its thickness decreases following a power-law profile along its length towards zero [5]. This ideal ABH geometry induces a unique phenomenon where the velocity of flexural waves gradually reduces and the travel time will prolong infinitely, leading to the elimination of wave reflections. This ideal design is not feasible in practical applications, as the edge of the ABH will always have a residual thickness. Thus, a viscoelastic damping layer [6, 7, 8] or piezoelectric layer [9, 10] can be applied to the ABH to mitigate the waves that will be reflected by the ABH edge. Several configurations of ABHs have been studied to understand its capabilities in vibration mitigation [11, 12], sound absorption [13, 14], and energy harvesting [15, 16], either embedded into the main structure [17, 18] or as attached vibration dampers [19, 20, 21]. Many of these configurations and works have been reviewed by Pelat et al. [22] in their review of the theory and applications of ABHs.

Considering ABHs embedded in a plate, Feurtado and Colon [23] investigated the use of wavenumber transform analysis to design and optimise ABHs in structures for vibration reduction and sound radiation control. This analysis allowed them to visualize and quantify the changes in bending wave speed, vibration amplitude, and energy dissipation due to the ABH effect. The re-

sults showed that when the ABH dynamics dominate the system response it could lead to lower vibration and sound radiation levels. This was attributed to the redistribution of supersonic bending waves into subsonic wavenumbers. Bowyer and Krylov [24] conducted an experimental analysis to investigate the capability of circular ABHs in reducing the acoustic response when compared with uniform plates. They compared the acoustic power response of a plate embedded with several circular ABHs and a central hole, to that of a uniform reference plate. Both plates were subjected to harmonic excitation through a point force. It was noted that while the vibration amplitudes at the centers of the ABHs were increased, the overall plate vibration was reduced and led to a mitigation in the sound radiation. This was ascribed to the synergistic impact of the ABH indentations and the acoustic short-circuiting resulting from the presence of the central hole. Deng et al. [25] utilized the wave finite element (FE) model to study the capability of embedded ABH in a cylindrical shell structures to reduce BF bending waves when subjected to a ring excitation. They investigated the BF passbands and stopbands in both uniform and ABH-embedded infinite cylindrical shells, demonstrating how ABHs can significantly alter these bands. The authors highlighted that while ABHs enhance vibration damping, they also reduce the shell's stiffness. In most applications this could be a disadvantage of embedded ABHs. To overcome this disadvantage, Zhang et al. [26] proposed ABH indentations with reinforcing stiffeners in a plate. Using a symplectic space wave propagation model, they showed that the ABH could still mitigate the plate's vibration, but the results indicated the mitigation effectiveness decreased due to the addition of reinforcements highlighting the limitation of embedded ABHs. Efforts to address this constraint have led to the emergence of additive ABHs, with initial investigations conducted following the concept's inception in Zhou et al. [19] work.

Zhou et al. [19] investigated the use of ABH as a dynamic vibration absorber (DVA). The approach combines DVA and waveguide absorber (WGA) principles, requiring no complex tuning and no variations in the host structure. They considered the vibration response of a beam as a benchmark solution, and employed numerical simulations using the FEM and experiments to demonstrate the ABH-DVA effectiveness in reducing vibration amplitudes at multiple resonance frequencies of the host structure across a broad frequency range. In a similar approach, Ji et al. [27] studied a 2D circular ABH-DVA to mitigate vibrations in plate structures utilizing the FE simulations and experimental results. It was shown that the 2D ABH-DVA significantly lowers

resonant peaks across a broad frequency range. This effect was attributed to dynamic interaction of the DVA and enhanced damping due to the energy trapping inherent in ABHs. Li et al. [28] investigated the efficacy of a vibration absorber that integrates the ABH effect with vibro-impact mechanisms, aimed at enhancing low-frequency vibration attenuation. Their study employed both numerical and experimental methodologies, using an FE model to simulate the dynamics of the absorber applied to a honeycomb panel, alongside conducting parametric studies to refine the design variables such as impact mass and stiffness. It was shown that the vibro-impact ABH absorber significantly mitigates vibrations across a broad frequency spectrum by efficiently transferring energy from lower to higher frequencies where it was dampened by the ABH-DVA. Deng et al. [29] also observed a wide vibration damping across a broad frequency range when studying ABH pillars attached to a plate excited by a point force using the Rayleigh–Ritz method. Their results highlighted the capability of attached ABHs in mitigating the vibration response of a host structure. To the best of the author's knowledge, to date there is no work in literature that investigate the vibroacoustic response of the ABH-DVA concept in fluid loaded structures. Moreover, it is unknown how implementing ABHs in a stiffened structure will affect the generation and propagation of BF waves in the structure.

In this work, ABHs are embedded in the plate's stiffeners, providing an excellent passive control strategy for stiffened structures without compromising the structural integrity of the host structure. This work also develops a semi-analytical model of a fluid-loaded infinite plate with ABH-shaped stiffeners. In the proposed formulations, the stiffeners' translational and rotational dynamic stiffnesses are initially obtained from an FE model in COMSOL Multiphysics™, which allows the modelling of complex stiffener shapes. The stiffeners' dynamic stiffnesses are then coupled with an analytical model of the infinite fluid-loaded plate in the wavenumber domain. The semi-analytical model provides an efficient computational tool that allows one to study how ABH stiffeners damp the BF travelling waves in the structure and their propagations as noise to the far field. This paper is organised as follows. In Section 2, we introduce the development of the semi-analytical model, and subsequently how to obtain the dynamic stiffnesses using the FEM. The section concludes with the method to obtain the Bloch-Floquet passbands considering the given stiffened structure. Section 3 presents a verification study through the comparison of the results obtained from the semi-analytical model with those from an FE model in

COMSOL Multiphysics™. A comparison between the vibroacoustic response of the system with rectangular and ABH stiffeners is presented to examine the effectiveness of the ABH stiffeners in reducing the BF wave propagation. The effects of adding damping layers to the stiffeners and the distance between stiffeners on the vibroacoustic response of the fluid-loaded plate with rectangular or ABH stiffeners are also presented. Finally, the conclusions are presented in Section 4.

2. Semi-analytical formulation

In this section, we introduce a semi-analytical formulation to model the vibroacoustic response of an infinite heavy-fluid loaded plate with ABH stiffeners. While the formulation can be applied to stiffeners with various cross-sections, as they are represented by a FEM, our focus is predominantly on exploring its applicability and effectiveness in the context of ABH stiffeners. The schematic diagram of the system is shown in Fig. 1, where, a 2D periodically distributed array of identical stiffeners is coupled with an infinite heavy fluid-loaded thin plate extending along the x-axis. $x = nd$ and n is an integer ($\mathbb{Z}$) indicating the stiffener's number, and d is the distance between them, as shown in Fig. 1. The stiffeners are assumed to have rigid connections with the plate. The plate of thickness h is considered to be excited by a point force F_0 at a position (x_0), and it is in contact with a heavy fluid (water) on one side in the half space Ω. Herein, $h = 0.010$ m and the fluid density ρ_f and sound speed c_f are 1000 kg/m^3 and 1500 m/s, respectively.

For the purposes of the following developments, let us omit the harmonic time dependence represented by $e^{\mathrm{j}\omega t}$, where ω is the excitation frequency in rad/s and j is the imaginary unit. Considering the Love-Kirchhoff assumptions, the equation of motion of the fluid loaded stiffened plate can be written as [30],

$$\begin{aligned} D\nabla^4 W(x,\omega) - \omega^2 \rho_\mathrm{s} h W(x,\omega) = {} & F_0 \delta(x - x_0) - p(x,\omega,0) \\ & - \sum_{n\in\mathbb{Z}} F(x,\omega)\,\delta(x - nd) \\ & + \sum_{n\in\mathbb{Z}} \frac{\partial}{\partial x}\left(M(x,\omega)\,\delta(x - nd)\right), \end{aligned} \tag{1}$$

where W, D and ρ_s are the plate's displacement, complex flexural rigidity and mass density, respectively. $p(x,\omega,0)$ is the wall pressure due to the

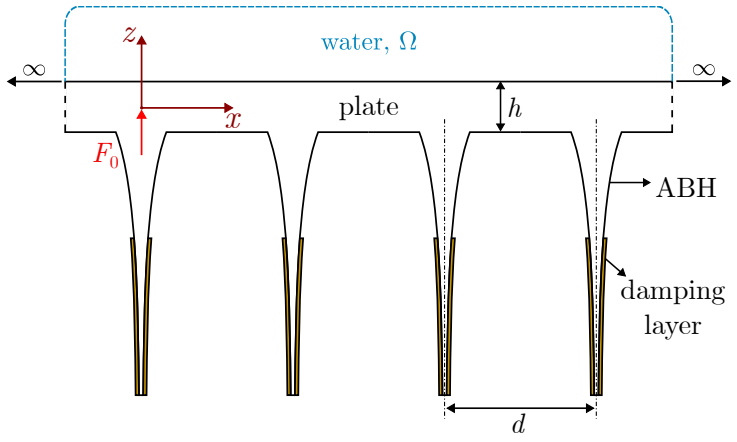

Figure 1: Schematic of an infinite heavy fluid-loaded plate with periodic ABH stiffeners.

fluid loading. The Dirac delta function is presented by δ. $F(x,\omega)\,\delta(x-nd)$ and $M(x,\omega)\,\delta(x-nd)$ are respectively the force and moment distributions related to the interaction between the plate and the nth stiffener. Assuming displacement continuity between the plate and stiffeners, the force and moment at their interface can be expressed as,

$$F(x,\omega) = T_{\mathrm{s}}(\omega)\, W(x,\omega), \tag{2}$$

$$M(x,\omega) = R_{\mathrm{s}}(\omega)\, \frac{\partial W}{\partial x}(x,\omega), \tag{3}$$

in which, T_{s} and R_{s} are the stiffener's translational and rotational dynamic stiffnesses, respectively. The numerical process for calculating these functions are provided in Section 2.2.

The acoustic pressure $p(x,\omega,z)$ in the fluid domain satisfies:

- The Helmholtz equation in the half space Ω occupied by the fluid,

$$\nabla^2 p(x,\omega,z) + k_{\mathrm{f}}^2 p(x,\omega,z) = 0\,,\ \forall (x,\omega,z) \in \Omega, \tag{4}$$

  where ∇ is the Nabla operator and k_{f} is the acoustic wavenumber.

- The Euler equation at the interface between plate and the fluid is given by,

$$\rho_{\mathrm{f}}\omega^2 W(x,\omega,0) = \frac{\partial p}{\partial z}(x,\omega,0). \tag{5}$$

- The Sommerfeld radiation conditions on a fictional infinite surface.

Applying space-Fourier transform to Eq. 1 yields [30]

$$\begin{aligned}\left[D\left(k_x^4\right)-\omega^2\rho_{\mathrm{s}}h\right]\widetilde{W}(k_x) =& F_0e^{-\mathrm{j}k_xx_0}-\widetilde{P}(k_x,0)\\ &-\frac{1}{d}T_{\mathrm{s}}\left[\sum_{n\in\mathbb{Z}}\widetilde{W}\left(k_x+\frac{2\pi n}{d}\right)\right]\\ &-\frac{k_x}{d}R_{\mathrm{s}}\left[\left(k_x+\frac{2\pi n}{d}\right)\sum_{n\in\mathbb{Z}}\widetilde{W}\left(k_x+\frac{2\pi n}{d}\right)\right],\end{aligned} \tag{6}$$

whereas applying the space-Fourier transform to Eqs. 4 and 5 yields

$$\begin{cases}\widetilde{P}(k_x,z)=\frac{\rho_{\mathrm{f}}\omega^2e^{\eta z}}{\eta}\widetilde{W}(k_x) & \text{if} \quad k_x\neq k_{\mathrm{f}},\\ \widetilde{P}(k_x,z)=C, \quad \widetilde{W}(k_x)=0 & \text{if} \quad k_x=k_{\mathrm{f}},\end{cases} \tag{7}$$

where C is a constant and $\eta=-\sqrt{k_x^2-k_{\mathrm{f}}^2}$. Finally, the spectral displacement and pressure can be written as [30, 31],

$$\widetilde{W}\left(k_x\right)=\widetilde{W}_0\left(k_x\right)\Gamma\left(k_x\right), \tag{8}$$

$$\widetilde{P}\left(k_x,z\right)=\widetilde{P}_0\left(k_x,z\right)\Gamma\left(k_x\right), \tag{9}$$

where, $\widetilde{W}_0\left(k_x\right)$ and $\widetilde{P}_0\left(k_x,z\right)$ are respectively the spectral displacement of the plate and spectral pressure for each value of z considering the plate without the stiffeners. k_x is the wavenumber in the x direction. The contributions of the stiffeners to the plate's vibration are given by $\Gamma\left(k_x\right)$. $\widetilde{W}_0\left(k_x\right)$ can be defined as,

$$\begin{cases}\widetilde{W}_0\left(k_x\right)=\frac{F_0e^{-\mathrm{j}k_xx_0}}{Z(k_x)} & \text{if } k_x\neq k_{\mathrm{f}},\\ \widetilde{W}_0\left(k_x\right)=0 & \text{if } k_x=k_{\mathrm{f}},\end{cases} \tag{10}$$

and the spectral pressure $\widetilde{P}_0\left(k_x,z\right)$ is given by,

$$\begin{cases}\widetilde{P}_0\left(k_x,z\right)=\frac{\rho_{\mathrm{f}}\omega^2F_0e^{-\mathrm{j}k_xx_0}e^{\eta z}}{Z(k_x)\eta} & \text{if } k_x\neq k_{\mathrm{f}},\\ \widetilde{P}_0\left(k_x,z\right)=F_0e^{-\mathrm{j}k_xx_0} & \text{if } k_x=k_{\mathrm{f}},\end{cases} \tag{11}$$

in which $Z\left(k_x\right)$ is the fluid-loaded plate dynamic stiffness defined by

$$Z\left(k_x\right) = Dk_x^4 - \rho_{\mathrm{s}}\omega^2 h + \mathrm{FL}, \tag{12}$$

where FL is the fluid loading term,

$$\mathrm{FL} = \frac{\rho_{\mathrm{f}}\omega^2}{\eta}. \tag{13}$$

The stiffeners contribution $\Gamma(k_x)$ is given by the following expression

$$\Gamma = \frac{\gamma_1 - \gamma_2 - \gamma_3}{\gamma_4 - \gamma_5}, \tag{14}$$

where,

$$\begin{cases} \gamma_1 = \frac{1}{d^2} T_{\mathrm{s}} R_{\mathrm{s}} S_1 \left(S_1 - \widehat{S}_1\right), \\ \gamma_2 = \left(1 + \frac{1}{d} R_{\mathrm{s}} S_2\right) \left[1 + \frac{1}{d} T_{\mathrm{s}} \left(S_0 - \widehat{S}_0\right)\right], \\ \gamma_3 = \frac{1}{d} k_x R_{\mathrm{s}} \left[\frac{1}{d} T_{\mathrm{s}} \left(\widehat{S}_0 S_1 - S_0 \widehat{S}_1\right) - \widehat{S}_1\right], \\ \gamma_4 = \frac{1}{d^2} T_{\mathrm{s}} R_{\mathrm{s}} S_1^2, \\ \gamma_5 = \left(1 + \frac{1}{d} R_{\mathrm{s}} S_2\right) \left(1 + \frac{1}{d} T_{\mathrm{s}} S_0\right), \end{cases} \tag{15}$$

in which,

$$S_p = \sum_{n \in \mathbb{Z}} \frac{\left(k_x + \frac{2\pi n}{d}\right)^p}{Z\left(k_x + \frac{2\pi n}{d}\right)}, \ \widehat{S}_p = \sum_{n \in \mathbb{Z}} \frac{\left(k_x + \frac{2\pi n}{d}\right)^p e^{-\mathrm{j}\frac{2\pi n}{d} x_0}}{Z\left(k_x + \frac{2\pi n}{d}\right)}, \tag{16}$$

where S_p and $\widehat{S}_p$ are associated with the stiffener number n and spacing between stiffeners d, considering $p = 0, 1, 2$. Finally, the spectral displacement and pressure in the wavenumber space can be analytically calculated from Eqs. 8 and 9, respectively.

2.1. Estimation of the vibratory field and sound power

As an indicator of the plate vibration, we can define the mean quadratic plate velocity on the plate section $[0, L]$ as [32],

$$\langle v^2 \rangle = \frac{\omega^2}{L} \int_0^L |W(x, \omega)|^2 dx, \tag{17}$$

where L is a distance from the excitation point. For the numerical application, the plate length L is equivalent to the distance covering the first 15 stiffeners ($L = 15d$). The displacement $W(x, \omega)$ can be estimated from the inverse discrete Fourier transform (IDFT) of the spectral displacement $\widetilde{W}(k_x)$ given by Eq. 8. Also in order to investigate the vibrational response, the transmissibility can be obtained considering the surface of the plate covering n stiffeners. The transmissibility is given by

$$\mathrm{T}_n = \frac{w_n^2}{w_0^2}, \tag{18}$$

in which, w_n and w_0 are the displacement at the n^{th} stiffener and at the stiffener at source, respectively. The transmissibility results presented in this paper consider $n = 15$.

The total acoustic power can be deduced using formulations exclusively dependent on the spectral wall pressure or displacement as Eq. 7 holds [33]. The radiated sound power exclusively dependent on the pressure can be written as follows,

$$\mathit{\Pi} = \frac{1}{4\pi\rho_{\mathrm{f}}\omega} \int_{k\in\Omega_a} -\eta|\widetilde{P}(k_x, 0)|^2 dk, \tag{19}$$

where, $\Omega_a = \{k_x \in \mathbb{R}, |k_x| \leq k_{\mathrm{f}}\}$ does not consider subsonic waves that do not propagate to the far-field and $\widetilde{P}(k_x, 0)$ is the spectral pressure given by Eq. 9 when $z = 0$. It should be noted that structural damping is introduced in the stiffened plate by considering complex Young's modulus. In Section 3.1, the present numerical results will be verified against those obtained from an FE model. Since in the FE model, only the sound power from a finite length of the stiffened plate can be obtained, to be able to conduct the verification study, the radiated sound power from a finite length of the plate should be defined. Similar to the mean quadratic velocity, the sound power ($\mathit{\Pi}_L$) can be calculated in the spatial domain considering a finite length of the plate as follows

$$\mathit{\Pi}_L = 1/2 \int_0^L \Re[p(x, \omega, 0)v^*(x, \omega)]dx, \tag{20}$$

in which, v^* is the complex conjugate of the plate's velocity $v(x, \omega)$, and $\Re$ is the real part of the complex number. IDFTs are applied on the spectral responses of the semi-analytical model to obtain the velocity $v(x, \omega)$ and wall pressure $p(x, \omega, 0)$ in the spatial domain.

2.2. Numerical calculation of the dynamic stiffness of the stiffeners

To account for the stiffeners contribution to the plate's dynamic behavior, we must determine their translational and rotational dynamic stiffnesses as delineated in Eqs. 2 and 3. Herein, an FE model of the stiffeners as illustrated in Fig. 2(a) is used to evaluate their dynamic stiffnesses. The FE model follows the mesh and element sizes described in Section 3.1, and is modeled using Solid Mechanics module in COMSOL Multiphysics™. Based on the initial assumption that the stiffeners have rigid connections with the plate, herein, the stiffeners are considered to have a Rigid Connector at the top edge where the force $F_{\mathrm{s}}(\omega)$ and moment $M_{\mathrm{s}}(\omega)$ are applied at the point B.

The schematic to obtain the translational and rotational dynamic stiffenesses is presented in Fig. 2(b). More precisely, the translational dynamic stiffeness $T_{\mathrm{s}}(\omega)$ is obtained by the ratio between the force $F_{\mathrm{s}}(\omega)$ applied at the point B and the resulting displacement $W_{\mathrm{s}}(\omega)$. Similarly, the rotational dynamic stiffeness $R_{\mathrm{s}}(\omega)$ can be obtained by the ratio between the moment $M_{\mathrm{s}}(\omega)$ applied at point B and the rotational response θ.

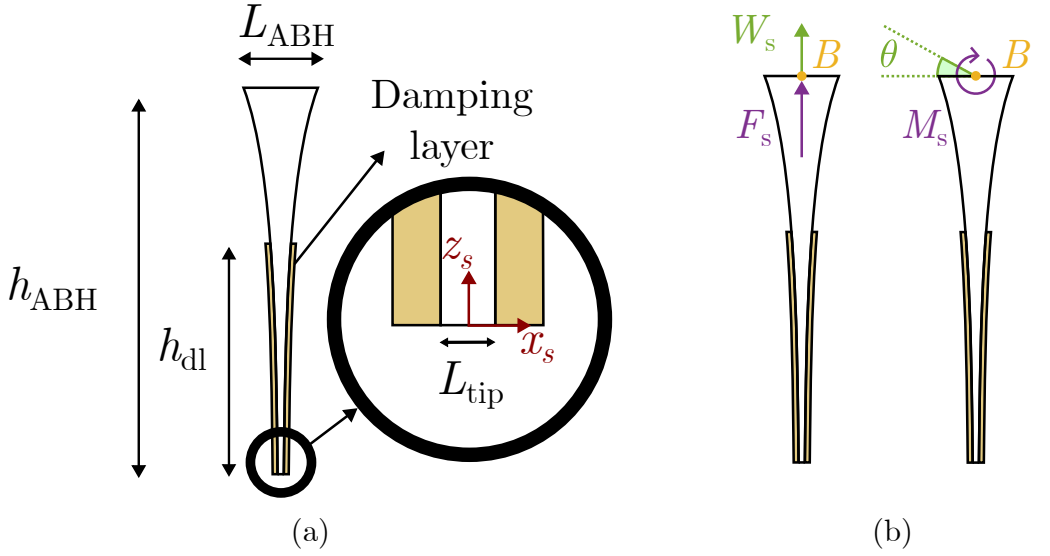

Figure 2: Schematics of (a) the ABH modeled by the FE and (b) the applied force and the moment to obtain the dynamic stiffness.

As shown in Fig. 2, the ABH stiffener considered in the following sections utilizes damping layers to mitigate the reflected waves at the tip which mimics

the ideal ABH as outlined in Ref. [34]. The correlation between the length of the ABH (L_{ABH}) and the local thickness (h_{ABH}) follows the power law curve expressed as $h_{\mathrm{ABH}}(z_{\mathrm{s}}) = \alpha z_{\mathrm{s}}^2 + h_{\mathrm{tip}}$, where α represents the power-law constant, h_{tip} is the tip thickness of the ABH, and z_{s} is the distance along L_{ABH} considering the local coordinate system (x_s, z_s).

2.3. Bloch-Floquet propagating waves

In the introduction, it was established that the passbands of the BF waves are associated with high levels of vibroacoustic responses. Therefore it is relevant to determine the BF passbands of the analysed system, in order to study how different stiffeners can modify the wave propagation characteristics within these frequency ranges and influence the radiated noise. The BF propagating waves can be identified by finding the real roots k^{BF} of the dispersion equation, corresponding to the denominator of Γ when the system is supposed conservative (i.e. without dissipation). If the k^{BF} are real, it implies that the BF waves are able to travel across the plate without attenuation. The dispersion equation, is given by

$$\Delta\left(k^{\mathrm{BF}}\right) = \gamma_4\left(k^{\mathrm{BF}}\right) - \gamma_5\left(k^{\mathrm{BF}}\right) = 0. \tag{21}$$

Previous research [35] has shown that when accounting for fluid loading in the formulation, it is not possible to derive explicit expressions for k^{BF}. As accounted by other studies [4, 31], an algorithm can be used to compute the real values for k^{BF}, and hereby the procedure is presented by the flowchart in Fig. 3. The objective is to identify the roots of Δ within the first Brillouin zone (i.e. $[0, \pi/d]$). The Brillouin zone is the fundamental region in reciprocal space that contains all unique wavenumbers which describe the wave behavior in a periodic medium, hence in this case only the first Brillouin zone needs to be examined [36, 37].

The process described in Fig. 3 is applied considering $\epsilon = 0.05$ and a discretisation of the interval $[0, \pi/d]$ with a resolution of 0.0001. After computing the passbands with the criterion $\Delta_{\mathrm{min}} < \epsilon$, the BF passbands are compared against the acoustic wavenumber k_{f} to determine if they are radiating ($k^{\mathrm{BF}} \leq k_{\mathrm{f}}$) or non-radiating ($k^{\mathrm{BF}} > k_{\mathrm{f}}$). It should be emphasized that Δ should be calculated for the conservative system. This means that the damping should be excluded from the system. Therefore, only the real parts of the Young's modulus and fluid loading term should be considered for computing passbands and stopbands.

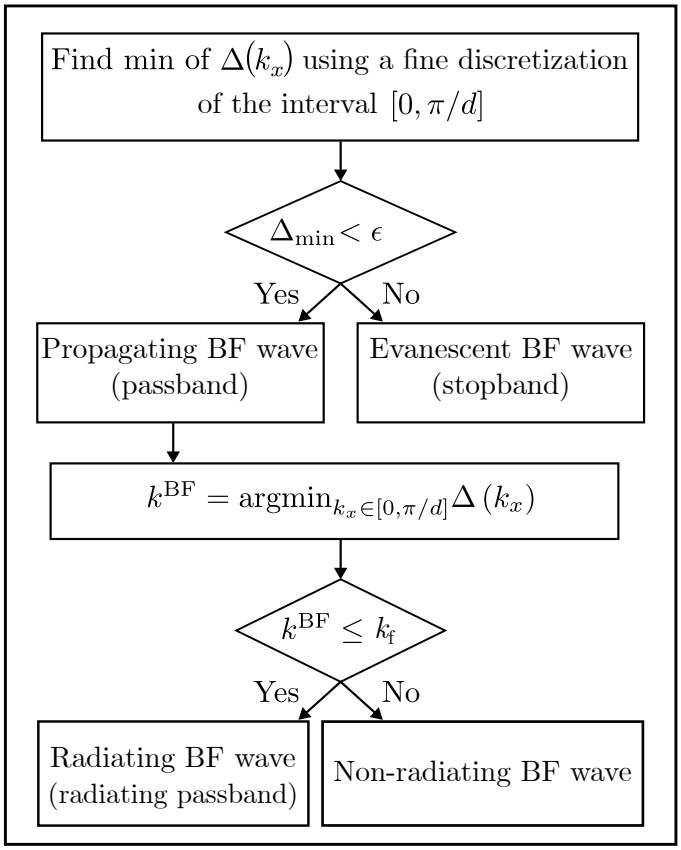

Figure 3: Algorithm to obtain the BF propagating waves considering a two-dimensional model.

3. Results and discussion

In this section, we explore how the ABH stiffeners could be a substitute for the rectangular stiffeners to mitigate the vibroacoustic response. Let us assume that we have a fluid-loaded stiffened plate with periodic rectangular stiffeners each with an area of A and moment of inertia of I_0 at point of contact with the plate. We would like to replace the conventional rectangular stiffeners with equivalent ABH stiffeners that are designed to match the rectangular stiffener's area A and moment of inertia I_0 ensuring that both stiffeners have similar weight and static stiffness. Both rectangular and ABH stiffeners have identical material properties as the plate, as detailed in Table 1, their geometrical properties are also given in Table 2. Before we

proceed with the investigation using the semi-analytical model, we will first verify its accuracy in predicting the vibroacoustic response of the infinite heavy fluid-loaded plate with ABH stiffeners.

Table 1: Material properties of the structure and damping layer.

Parameters	Structure	Damping Layer
Young's modulus ($E_{\mathrm{s,dl}}$)	$210 \times 10^9\,(1 + \mathrm{j}\beta_{\mathrm{s}})$ Pa	$0.25 \times 10^9\,(1 + \mathrm{j}\beta_{\mathrm{dl}})$ Pa
Mass density ($\rho_{\mathrm{s,dl}}$)	7800 kg/m^3	950 kg/m^3
Poisson's ratio (ν)	0.3	0.3
Loss factor ($\beta_{\mathrm{s,dl}}$)	0.005	0.5

Table 2: Geometrical properties of the stiffeners.

Parameters	Rectangular stiffener	ABH stiffener
Thickness ($h_{\mathrm{r,ABH}}$)	0.010 m	0.016 m
Length ($L_{\mathrm{r,ABH}}$)	0.100 m	0.164 m
Tip thickness (h_{tip})	-	0.0005 m
Damping layer length (L_{dl})	$0.7L_{\mathrm{r}}$	$0.7L_{\mathrm{ABH}}$
Damping layer thickness (h_{dl})	0.003 m	0.003 m

3.1. Semi-analytical model verification

A MATLAB code was developed based on the formulation described in the previous section, and a corresponding 2D FE model was created, as depicted in the schematic shown in Fig. 4 using the commercial software COMSOL Multiphysics™. In the FE model, we utilized a perfectly matched layer (PML) to simulate the infinite plate. The PML serves as a synthetic absorbing layer, effectively dampening the waves as they propagate and minimizing any reflections at the boundary. Both models were used to generate vibroacoustic results to verify the semi-analytical model, considering the geometrical and material properties in Tables 1 and 2. Due to the limitation of the FE model to account for the infinite domain, the plate length L is considered to be the distance covering the first 15 stiffeners ($L = 15d$). The system is considered to be excited by a point force $F_0 = 1$ N at $x = 0$ m, and has ABH-shaped stiffeners.

The mean quadratic velocity (Eq. 17) and sound power (Eq. 20) response obtained using the semi-analytical model are compared against the response

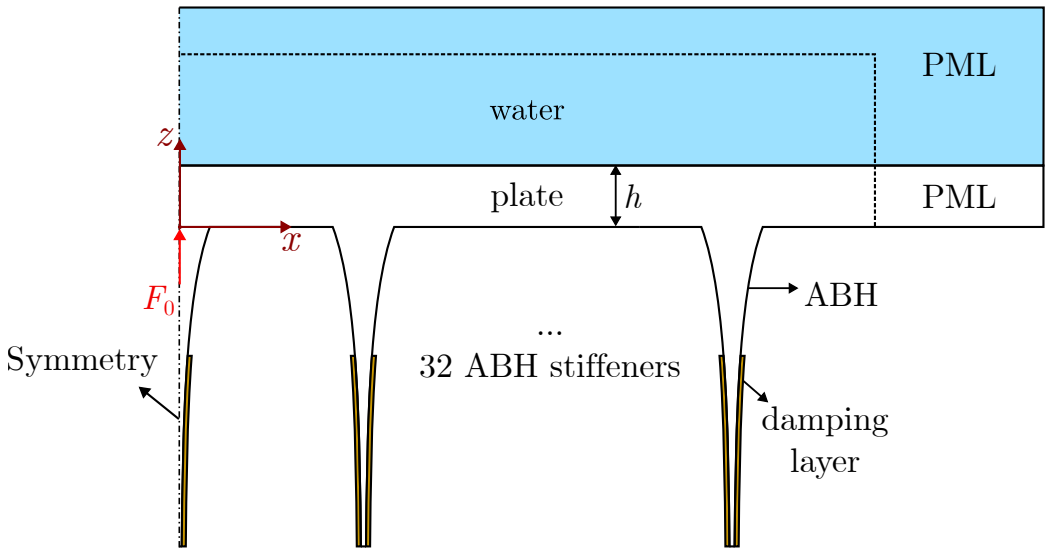

Figure 4: Schematic of the FE model of the infinite heavy fluid-loaded plate utilized in COMSOL Multiphysics™.

computed for the full FE model of the stiffened-plate-fluid system in COMSOL Multiphysics™ as shown in Fig. 5. In the FE model, we utilized a mapped mesh with element size determined by considering the criterion of 12 elements per wavelength. This specification was based on the wavelength at the tip of the ABH stiffener, corresponding to the highest frequency of interest, 5000 Hz. Based on a convergence study (results are not shown here), the PML size was set to 6 m, while the fluid layer above the structure was set to a height of 0.75 m. The vibration and acoustic responses are shown in Figs. 5(a) and (b), respectively. In both sets of results, multiple peaks are evident. These peaks originate from the BF waves and are associated with the passbands identified by the algorithm presented in Section 2.3. These results will be further discussed in the subsequent sections. As shown in Fig. 5, the results obtained by the semi-analytical model are in a good agreement with the response of the FE model, with a difference lower than 2 dB. Notably, the computational time required for the semi-analytical modeling to obtain the response was less than 1% of that required for the FE model.

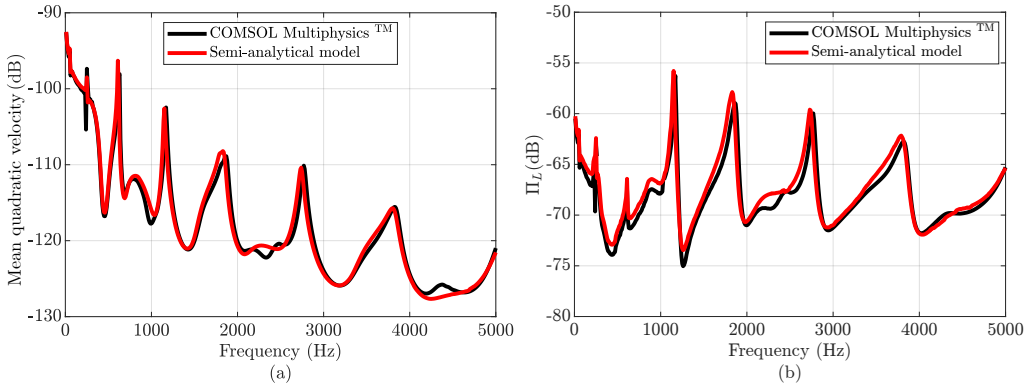

Figure 5: Comparison of the FE model using COMSOL Multiphysics™ (black line) and the semi-analytical formulation (red line) in terms of (a) mean quadratic velocity defined by Eq. 17 (dB, ref. 1 m^2 s^{-2}), and (b) radiated sound power defined by Eq. 19 (dB, ref. 1 W).

3.2. Vibration response

In order to verify if the ABH stiffeners could substitute the rectangular stiffeners to control the vibroacoustic response, let us investigate how the damping layers and the ABH-shaped stiffener affect the vibratory response. It is well known that when designing an ABH, it is necessary to account for the ABH's cut-on frequency ($f_{\text{cut-on}}$). By definition, the cut-on frequency of ABH is a critical parameter that delineates the threshold at which the ABH begins to effectively propagate and absorb flexural waves, marking the commencement of its damping capabilities [22]. The cut-on frequency is dependent on the geometry and material properties, and for the ABH stiffener considered in this work is defined as follows [38],

$$f_{\text{cut-on}} = \frac{\pi h_{\text{ABH}}}{4L_{\text{ABH}}^2}\sqrt{\frac{E_{\text{s}}}{3\rho_{\text{s}}}}, \tag{22}$$

in which E_{s} is the Young's modulus of the stiffeners. Based on Eq. 22 and the ABH parameters outlined in Table 2, the cut-on frequency for this shape is identified at 1392 Hz.

An initial analysis is made in relation to the addition of the damping layers to the two stiffener shapes. The stiffeners are modeled in COMSOL as described in Section 2.2. Fig. 6 shows the rotational receptance ($|R_s^{-1}|$) of

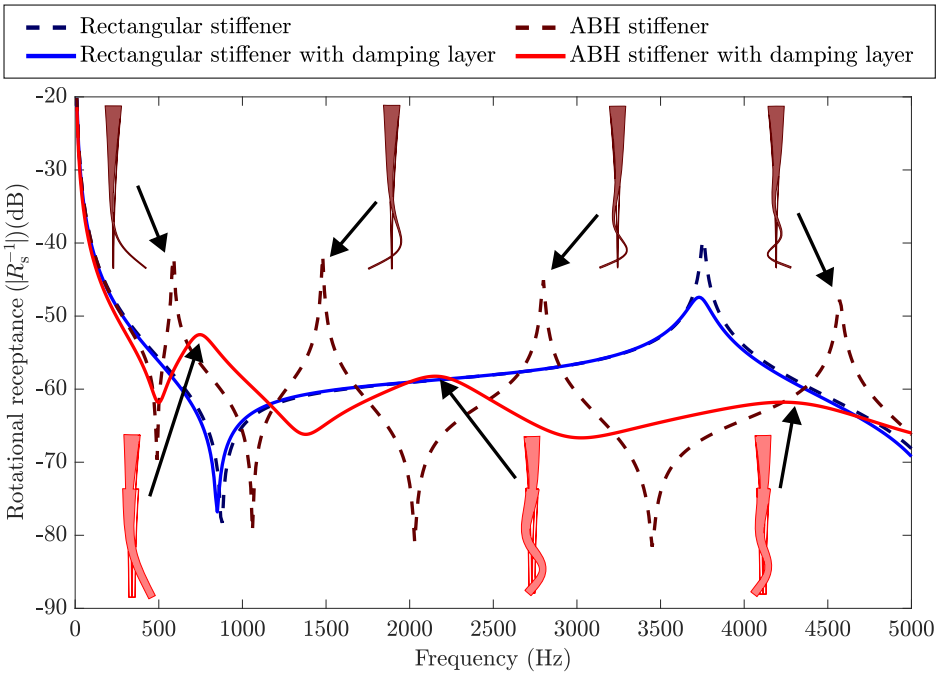

Figure 6: Comparison of the rotational receptance ($|R_s^{-1}|$) between rectangular and ABH stiffeners. Mode shapes of the ABH stiffener with damping layers are highlighted in red at their respective resonance frequencies. (dB, ref. 1 rad.N^{-1}.m^{-1}).

the rectangular and ABH stiffeners with and without damping layers. Due to the identical static stiffness of both stiffeners, at low frequencies the rotational receptance is similar across all cases. For the rectangular stiffener, the addition of the damping layers causes a slight frequency shift around 790 Hz and a slight attenuation of the peak around 3700 Hz. In contrast, the ABH stiffener is greatly influenced by the damping layers addition. Specifically, the rotational receptance of the ABH stiffener with damping layers shows less pronounced resonance peaks and a shift to higher frequencies, despite the added mass from the damping layers. The damping layer not only adds inertia but also contributes to the stiffness of the ABH, especially when its thickness is significant compared to the ABH thickness at the tip. The ABH stiffener with damping layers has 3 resonance frequencies in the analysed spectrum range, whilst the ABH stiffener without damping layers has 4 resonance frequencies in the same spectrum. The resonance frequencies and respective mode shapes are also shown in Fig. 6. The flexural natural

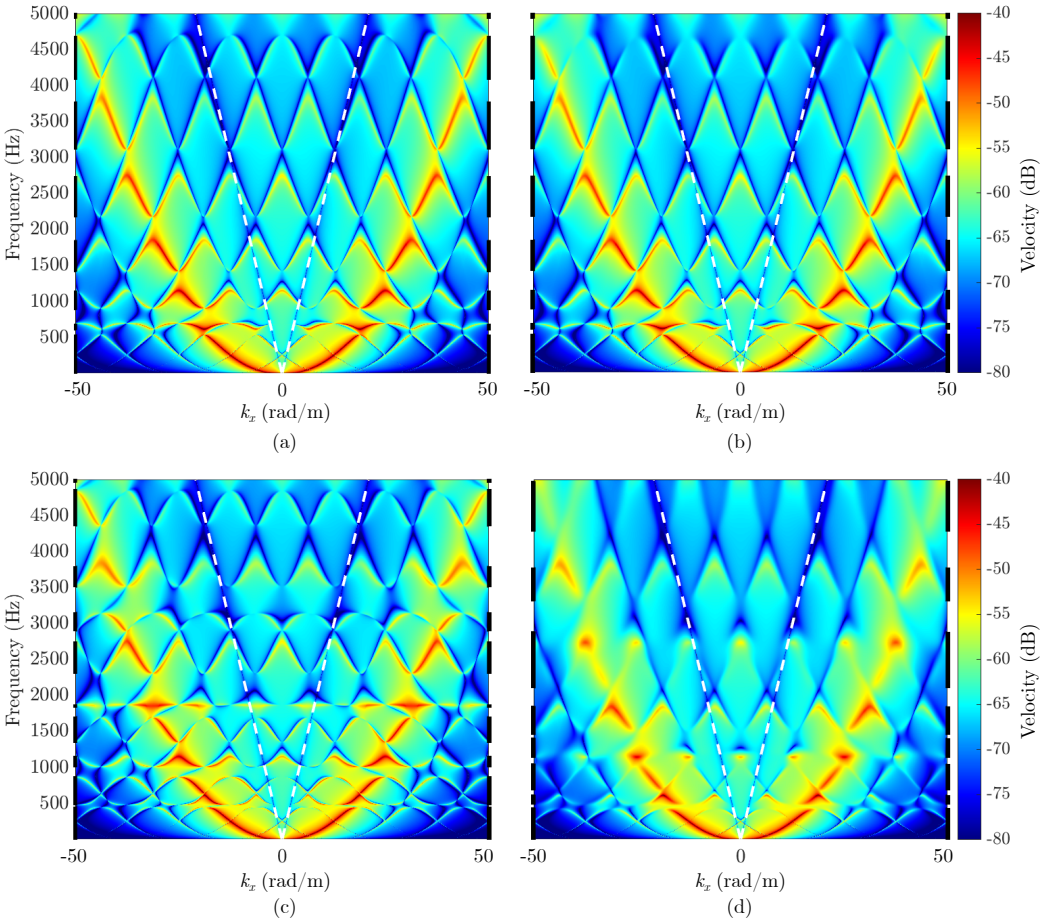

Figure 7: Wavenumber spectrum of the fluid-loaded plate's velocity (a) with rectangular stiffeners, (b) with rectangular stiffeners and damping layers, (c) with ABH stiffeners without damping layers and (d) with ABH stiffeners and damping layers. The acoustic wavenumber k_f is presented by the white dashed line. (dB, ref. 1 m.s^{-2}.N^{-1}).

frequency and mode shapes were obtained using COMSOL Multiphysics™ eigenfrequency analysis. The natural frequencies of the ABH stiffener with damping layers are 742 Hz, 2177 Hz, and 4310 Hz and they correspond to the resonance peaks in Fig. 6. Similarly, the natural frequencies of the ABH stiffener without damping layers are 585 Hz, 1479 Hz, 2798 Hz and 4572 Hz and they correspond to the resonance peaks in Fig. 6. One can note that, higher modes can be associated with a greater damping effect, leading to a damp-

ened rotational receptance spectrum without prominent resonance peaks and shifted to higher frequencies. This effect is evident from the distinct attenuation pattern of the ABH stiffeners with damping layers, compared to the ABH stiffeners without damping layers.

The wavenumber spectrum of the fluid-loaded plate's velocity of four different cases are presented in Fig. 7. The four cases are the fluid-loaded plate with (a) rectangular stiffeners, (b) rectangular stiffeners and damping layers, (c) ABH stiffeners without damping layers and (d) ABH stiffeners and damping layers. The acoustic wavenumber is presented by the white dashed line, and the respective passbands are given by the black bars in the y-axis at both edges of the spectrum. It can be observed from Fig. 7(a) and (b) that adding damping layers into the rectangular stiffeners does not significantly alter the system's vibrational response up to 4000 Hz. Above 4000 Hz, a slight mitigation is noticeable in the wavenumber spectrum causing a "blurry" effect in the color gradient of the amplitude. When comparing Figs. 7(c) and (d), it is noticeable that the addition of damping layers led to a greater mitigation effect in the system's response. The same blurry effect in the color gradient that once occurred smoothly for the rectangular-stiffened plate, here for the ABH-stiffened plate has a greater effect. The velocity response inside the acoustic triangle (i.e., $|k_x| \leq k_\mathrm{f}$) has slightly lower amplitudes when the damping layers are added, this is visible by the change from yellow to green in the color gradient. Now considering the two cases with damping layers, Fig. 7(b) and (d), it is clear that the ABH stiffeners present a lower amplitude response within the acoustic triangle and a blurry effect for the response above 450 Hz. For all the subsequent calculations, we will only consider stiffeners with the damping layers.

Fig. 8 shows the vibration behaviour of the plate with rectangular stiffeners and ABH stiffeners in terms of mean quadratic velocity and transmissibility. The passbands of the BF propagating waves are highlighted by the blue-shaded and red-shaded areas for the system with rectangular stiffeners and ABH stiffeners, respectively. The passbands were obtained using the algorithm presented in Section 2.3 considering the respective system with rectangular or ABH stiffeners. It is visible that the high amplitude response peaks are associated with the BF passbands as already established in the literature [4, 31].

Fig. 8(a) shows the mean quadratic velocity of the two analysed systems. It can be seen that the system with ABH stiffeners presents a lower response amplitude in almost the entire analysed frequency range reaching

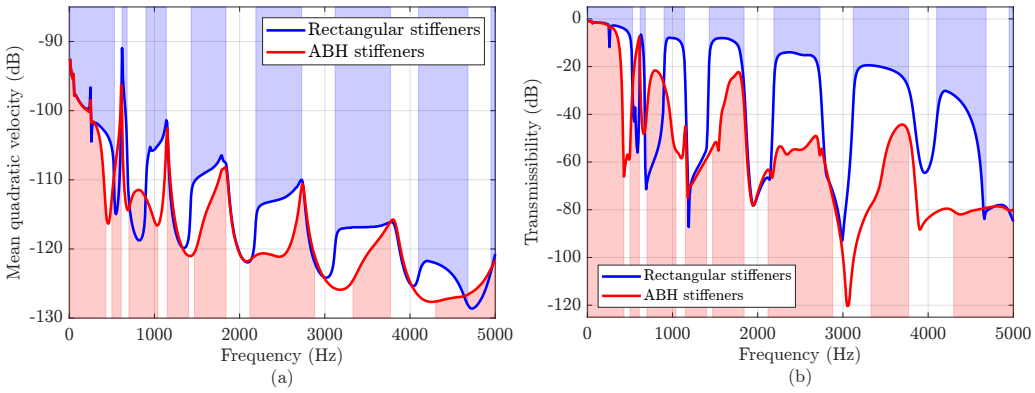

Figure 8: Comparison between the plate with rectangular stiffeners and ABH stiffeners in terms of (a) the mean quadratic velocity (dB, ref. 1 m^2 s^{-2}) and (b) transmissibility between the first 15 stiffeners.

up to 10 dB difference at 1500 Hz. The ABH-stiffened plate was able to mitigate the plate's velocity at a wide frequency range within the passbands as observed in four out of five passbands from 742 Hz to 4000 Hz. As frequencies approach the transition into stopbands the velocity amplitude increases, which indicates that the ABH is able to mitigate the propagation of the BF waves in the start of the passbands, but its effectiveness diminishes at frequencies towards the end of the passbands. Interestingly, the mitigation in the response occurs systematically above 742 Hz which is the first flexural natural frequency of the ABH stiffener with damping layers and although it is below the cut-on frequency. Considering the rectangular-stiffened plate, the noticeable vibration reduction begins above 4500 Hz caused by the damping layers as already shown in the wavenumber spectrum response (Fig. 7(b)). When both stiffened plates are inside a stopband the type of stiffeners has few influence in the mean quadratic velocity as observed in the stopbands around 2000 Hz and 3000 Hz. Similarly, Fig. 8(b) presents the transmissibility of the two stiffened plates. When observing the transmissibility comparison, it is visible that the ABH stiffeners were able to mitigate the vibrations, with an amplitude difference up to 60 dB at 3300 Hz and almost 50 dB at 4200 Hz when compared to the rectangular stiffeners. The vibration reduction within the passbands starts at 742 Hz which is consistent with the mean quadratic velocity results. In contrast to the latter, the passbands in the transmissibility response does not present the same pattern of high response amplitude

at each transition into stopbands. Unlike the ABH-stiffened plate, the transmissibility from the rectangular-stiffened plate maintain the high amplitudes for all passbands, with a partial attenuation in its last passband which is consistent with the results in the wavenumber domain (Fig. 7).

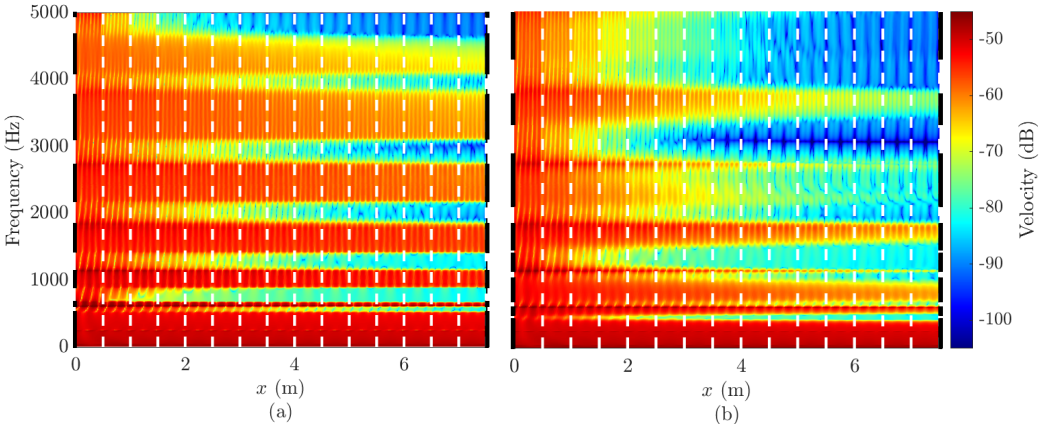

Figure 9: Spatio-spectra map of the plate's surface velocity (x, ω) considering the plate with (a) rectangular stiffeners and (b) ABH stiffeners. The stiffener's positions are presented by the white dashed lines and the passbands are presented by the black bars at the edge of each map. (dB, ref. 1 m.s^{-1}).

Fig. 9 shows the spatio-spectra map of the plate's surface velocity for the two cases. The stiffener's positions are presented by the vertical white dashed lines, and the respective passbands are presented by the black bars in the y-axis at each map's edge. Considering the spatio-spectra map of the surface velocity of the plate with rectangular stiffeners (Fig. 9(a)), the high amplitude within the passbands remains from the source at $x = 0$ m to the 15$^{\text{th}}$ stiffener at $x = 7.5$ m. In conformity with the previous results (Figs. 7 and 8) for the plate with rectangular stiffeners, the only passband that presents a high mitigation is the one above 4000 Hz, changing from orange to yellow-green, representing around 15 dB in difference. When observing Fig. 9(b) which presents the response of the plate with ABH stiffeners, the mitigation is greater in almost all the passbands. Considering the passbands from 2000 Hz to 5000 Hz, all three were lowered more than 20 dB after the 10^{th} stiffener, showing the strong mitigation capability of the ABH stiffener. This is observed by the high vibration decaying rate changing the color gradient from red to green/blue within the 2000 Hz - 5000 Hz frequency range. The pass-

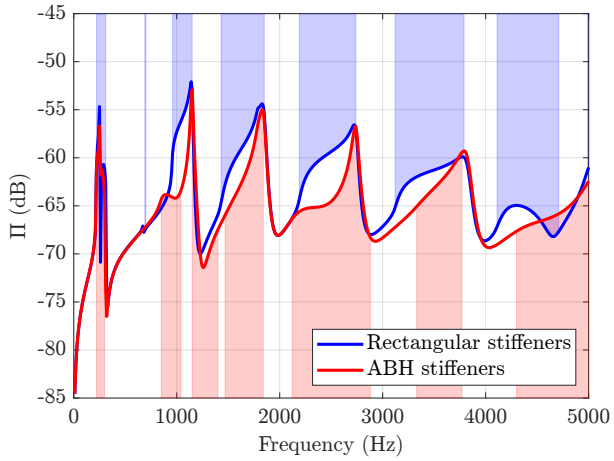

Figure 10: Radiated sound power of the rectangular-stiffened plate and the ABH-stiffened plate. The blue-shadded and red-shadded areas represent the radiating passbands of the propagating BF waves for the system with rectangular stiffeners and ABH-stiffeners, respectively. (dB, ref. 1 W).

bands bellow 2000 Hz, were partially mitigated but a peak still remains after the 15 stiffeners, showing again that the effectiveness of the ABH stiffener diminishes at frequencies towards the end of the passbands. The findings in this section confirm that the vibration response can be effectively mitigated by replacing common rectangular stiffeners with ABH stiffeners, leading us to investigate how the acoustic response is affected.

3.3. Radiated sound power

The radiated sound power of the infinite fluid-loaded plate with rectangular and ABH stiffeners are presented in Fig. 10, using Eq. 19. The radiating passbands of the BF propagating waves are highlighted by the blue-shaded and red-shaded areas for the system with rectangular stiffeners and ABH stiffeners, respectively. Fig. 10 shows that the highest amplitudes are within the BF passbands. Similarly to the vibration response, the sound power from the system with ABH stiffeners has a lower amplitude in almost the entire frequency range. The ABH-stiffened plate presents reduced sound power amplitude for frequencies above 742 Hz, which is consistent with the vibration results. This is observed when comparing the difference in amplitudes between the two response curves within the passbands for the results above

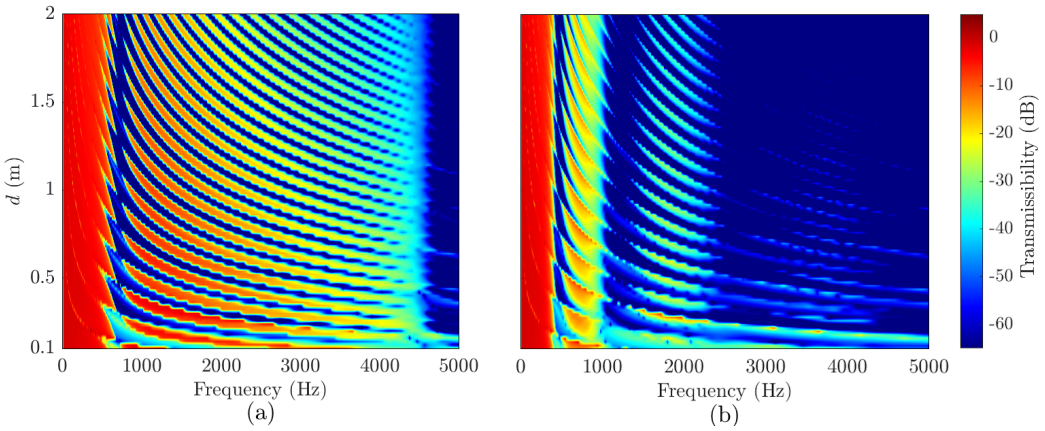

Figure 11: Transmissibility with respect to the stiffener spacing, considering a plate with (a) rectangular stiffeners and (b) ABH stiffeners.

742 Hz. The response from the ABH-stiffened plate presents a lower amplitude up to 7 dB at 1000 Hz and 2400 Hz. It is evident that the response amplitudes are higher at the end of almost all pass bands, indicating partial mitigation of the radiated sound power, similar to the mean quadratic velocity results. It can be highlighted that the attenuation induced by the use of ABH stiffener instead of rectangular stiffener is less pronounced for the radiated sound power than that of the mean quadratic velocity. However, this partial mitigation of the radiated sound power remain of interest for the practical applications.

3.4. Vibroacoustic response with respect to the stiffener spacing

To investigate the effect of the distance between stiffeners on the vibroacoustic response of the ABH stiffened plate in comparison to the rectangular stiffened one, this section considers the results for transmissibility and radiated sound power for various values of d. With a larger distance between stiffeners, additional passbands and consequently peaks are introduced to the vibration response. This can be visualised in Fig. 11, which presents transmissibility maps for (a) rectangular stiffeners and (b) ABH stiffeners with respect to the distance between stiffeners. The horizontal axis denotes the frequency range from 0 Hz to 5000 Hz, while the vertical axis represents the stiffener spacing denoted by d in meters. The color gradient, quantifying transmissibility in decibels (dB), transitions from high (red) to low

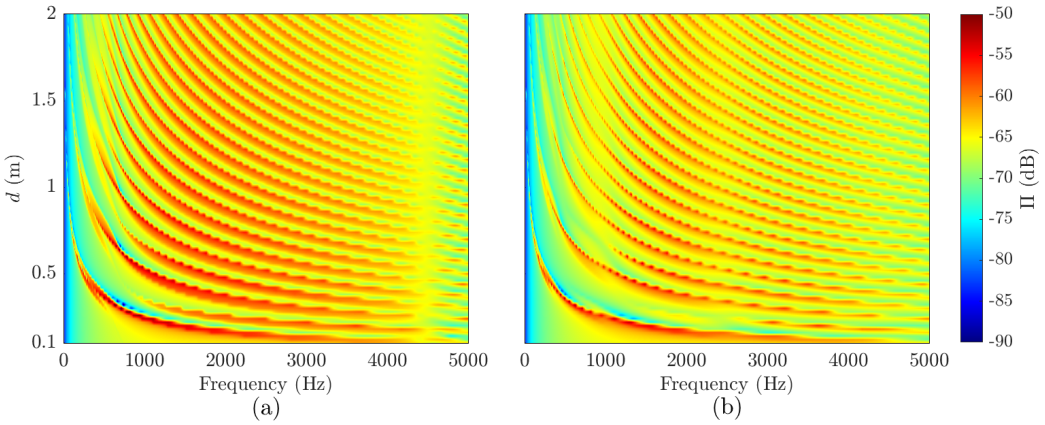

Figure 12: Radiated sound power with respect to the distance between stiffeners, considering a plate with (a) rectangular stiffeners and (b) ABH stiffeners. (dB, ref. 1 W).

(blue) amplitude values. The transmissbility response from the system with rectangular stiffener shows that there is a wide frequency band (1000-4000) with a small mitigation of the vibration energy from the source to the 15^{th} stiffener. The results are consistent to the ones presented in the previous section, that shows the effect of damping layers for results above 4000 Hz. The transmissibility response for this system, is characterized by distinct, periodic bands of high transmissibility indicated by pronounced amplitude peaks. Conversely, the map presented in Fig. 11(b) depicts the system utilizing ABH stiffeners, demonstrating a significant attenuation of transmissibility across the frequency spectrum. The ABH stiffeners exhibit an irregular pattern of reduced transmissibility, especially evident in the extended regions of low transmissibility (above 2000 Hz considering the distance d from 0.1 m to 1.5 m). The patterns are not regular as that in the rectangular-stiffened plate where we observe a clear pattern up to 4500 Hz. This behaviour could be due to the enhanced vibration damping capabilities of the ABH, acting as an intensifier of the damping layers effect since the rectangular-stiffened plate exhibits the same irregular pattern at the frequency bands where we observe the damping layers effect (above 4500 Hz). When comparing Fig. 11(a) and (b), the disparity between the two maps underscores the efficacy of ABH stiffeners in mitigating vibration transmission and highlights their potential vibration mitigation in stiffened structures.

Similarly to the transmissibility response, Fig. 12(a) presents the radiated sound power response from a structure with rectangular stiffeners, where we observe pronounced periodic bands of high sound power, which become denser as the spacing between stiffeners increases denoting the same direct correlation between, stiffener spacing and the greater number of peaks. This configuration shows a similar pattern of high amplitudes as the transmissibility response (Fig. 11) and a distinct dampening effect around 4500 Hz for all the considered distances d. In contrast, Fig. 12(b) depicts the system with ABH stiffeners. Notably, the ABH stiffeners show a marked reduction in sound power levels across the examined frequency spectrum, demonstrated by fewer and less intense bands of high radiated sound power. This reduction in the response amplitude is visible across all considered d, thereby showcasing the ABH stiffeners' superior damping properties. The visual comparison between the two maps suggests the same partial reduction of the BF waves contribution (since it is directly associated with the high levels of vibroacoustic response). This is noted by the width of each peak (red curved area) that are less prominent in the response of the ABH-stiffened plate. These findings shows that even with a larger number of peaks (and larger distance between stiffeners) the ABH stiffeners are able to mitigate the vibroacoustic response.

4. Conclusions

In this work, a semi-analytical formulation for the vibroacoustic response of a 2D infinite fluid-loaded plate with ABH stiffeners was developed. The stiffeners' characteristics were defined by their translational and rotational dynamic stiffnesses obtained through an FE model. These dynamic stiffnesses were then coupled with an analytical model of the infinite fluid-loaded plate in the wavenumber domain, allowing a detailed examination of vibroacoustic response and identification of the associated passbands and radiating passbands of the propagating BF waves for given stiffened plates. The proposed method is an efficient computational tool for examining the vibroacoustic behaviour of different designs of fluid-loaded plates with complex stiffeners.

Using the developed formulation, the effectiveness of implementing ABH stiffeners as a passive approach for attenuating the vibroacoustic response of an infinite heavy-fluid loaded plate subjected to a point force excitation was demonstrated. The ABH stiffeners were designed to have the same surface

area and moment of inertia (at the contact point) as those of conventional rectangular stiffeners to maintain the same static stiffness. The ABH damping effect was observed below the so-called cut-on frequency given in the literature. Notably, the systematic mitigation effect in the passbands and radiating passbands occurred consistently above the first flexural natural frequency of the ABH stiffener. It was also shown that the vibroacoustic responses of the plate with ABH stiffeners were significantly lower than those of the plate with rectangular stiffeners at the beginning of each passband. However, the predicted responses become almost the same at the end of each passband (beginning of the next stopband) when focusing on the mean quadratic velocity results. This effect was also visualised by the spatial-spectra maps, where the vibration response was plotted along the plate for different frequencies.

The analysis also showed that ABH stiffeners significantly reduce the radiated sound power over a broad frequency spectrum inside the radiating passbands, particularly above the first flexural natural frequency of the ABH stiffeners. While the attenuation effect on the radiating sound power is less pronounced than on mean quadratic velocity, the mitigation remains valuable for practical applications. These findings underscore the advantages of using ABH stiffeners over rectangular stiffeners for noise reduction in fluid-loaded plates.

References

[1] G. Eatwell, D. Butler, The response of a fluid-loaded, beam-stiffened plate, Journal of Sound Vibration 84 (3) (1982) 371–388.

[2] B. Mace, Periodically stiffened fluid-loaded plates, I: Response to convected harmonic pressure and free wave propagation, Journal of Sound Vibration 73 (4) (1980) 473–486.

[3] B. Mace, Periodically stiffened fluid-loaded plates, II: response to line and point forces, Journal of Sound Vibration 73 (4) (1980) 487–504.

[4] D. Martins, M. Karimi, L. Maxit, R. Kirby, Non-negative intensity for a heavy fluid-loaded stiffened plate, Journal of Sound and Vibration 566 (2023) 117891.

[5] M. Mironov, Propagation of a flexural wave in a plate whose thickness decreases smoothly to zero in a finite interval, Soviet Physics: Acoustics 34 (3) (1988) 318–319.

[6] V. Krylov, Laminated plates of variable thickness as effective absorbers for flexural vibrations, in: Proceedings of the 17th International Congress on Acoustics, Vol. 1, 2001, pp. 270–271.

[7] L. Tang, L. Cheng, H. Ji, J. Qiu, Characterization of acoustic black hole effect using a one-dimensional fully-coupled and wavelet-decomposed semi-analytical model, Journal of Sound and Vibration 374 (2016) 172–184.

[8] B. Austin, J. Cheer, Realisation of acoustic black holes using multi-material additive manufacturing, Frontiers in Physics 10 (2022) 1070345.

[9] Z. Wan, X. Zhu, T. Li, J. Fu, A method for improving wave suppression ability of acoustic black hole plate in low-frequency range, Thin-Walled Structures 182 (2023) 110327.

[10] Y. Zhen, H. Li, Y. Tang, Novel vibration control method of acoustic black hole plates using active–passive piezoelectric networks, Thin-Walled Structures 186 (2023) 110705.

[11] H. Li, C. Touzé, F. Gautier, A. Pelat, Linear and nonlinear dynamics of a plate with acoustic black hole, geometric and contact nonlinearity for vibration mitigation, Journal of Sound and Vibration 508 (2021) 116206.

[12] Y. Bao, Z. Yao, Y. Zhang, X. Hu, X. Liu, Y. Shan, T. He, Ultra-broadband gaps of a triple-gradient phononic acoustic black hole beam, International Journal of Mechanical Sciences 265 (2024) 108888.

[13] X. Li, Q. Ding, Sound radiation of a beam with a wedge-shaped edge embedding acoustic black hole feature, Journal of Sound and Vibration 439 (2019) 287–299.

[14] L. Ma, L. Cheng, Numerical and experimental benchmark solutions on vibration and sound radiation of an acoustic black hole plate, Applied Acoustics 163 (2020) 107223.

[15] H. Ji, Y. Liang, J. Qiu, L. Cheng, Y. Wu, Enhancement of vibration based energy harvesting using compound acoustic black holes, Mechanical Systems and Signal Processing 132 (2019) 441–456.

[16] H. Li, O. Doaré, C. Touzé, A. Pelat, F. Gautier, Energy harvesting efficiency of unimorph piezoelectric acoustic black hole cantilever shunted by resistive and inductive circuits, International Journal of Solids and Structures 238 (2022) 111409.

[17] L. Zhao, F. Semperlotti, Embedded acoustic black holes for semi-passive broadband vibration attenuation in thin-walled structures, Journal of Sound and Vibration 388 (2017) 42–52.

[18] L. Ma, L. Cheng, Sound radiation and transonic boundaries of a plate with an acoustic black hole, The Journal of the Acoustical Society of America 145 (1) (2019) 164–172.

[19] T. Zhou, L. Cheng, A resonant beam damper tailored with acoustic black hole features for broadband vibration reduction, Journal of Sound and Vibration 430 (2018) 174–184.

[20] H. Ji, N. Wang, C. Zhang, X. Wang, L. Cheng, J. Qiu, A vibration absorber based on two-dimensional acoustic black holes, Journal of Sound and Vibration 500 (2021) 116024.

[21] P. Liu, H. Huang, X. Wang, Q. Tang, X. Qi, S. Su, Z. Xiang, J. Hu, Acoustic black hole profiles for high-performance ultrasonic tweezers, Mechanical Systems and Signal Processing 188 (2023) 109991.

[22] A. Pelat, F. Gautier, S. C. Conlon, F. Semperlotti, The acoustic black hole: A review of theory and applications, Journal of Sound and Vibration 476 (2020) 115316.

[23] P. A. Feurtado, S. C. Conlon, Wavenumber transform analysis for acoustic black hole design, The Journal of the Acoustical Society of America 140 (1) (2016) 718–727.

[24] E. Bowyer, V. V. Krylov, Experimental study of sound radiation by plates containing circular indentations of power-law profile, Applied Acoustics 88 (2015) 30–37.

[25] J. Deng, O. Guasch, L. Maxit, L. Zheng, Reduction of bloch-floquet bending waves via annular acoustic black holes in periodically supported cylindrical shell structures, Applied Acoustics 169 (2020) 107424.

[26] S. Zhang, Q. Cheng, Y. Ma, Z. Deng, A symplectic analytical wave propagation model for forced vibration of thin plate with acoustic black hole indentation, Thin-Walled Structures 195 (2024) 111339.

[27] H. Ji, X. Zhao, N. Wang, W. Huang, J. Qiu, L. Cheng, A circular eccentric vibration absorber with circumferentially graded acoustic black hole features, Journal of Vibration and Acoustics 144 (2) (2022) 021014.

[28] H. Li, P. O'donoughue, F. Masson, A. Pelat, F. Gautier, C. Touzé, Broadband shock vibration absorber based on vibro-impacts and acoustic black hole effect, International Journal of Non-Linear Mechanics 159 (2024) 104620.

[29] J. Deng, N. Gao, X. Chen, B. Han, H. Ji, Evanescent waves in a metabeam attached with lossy acoustic black hole pillars, Mechanical Systems and Signal Processing 191 (2023) 110182.

[30] L. Maxit, Wavenumber space and physical space responses of a periodically ribbed plate to a point drive: A discrete approach, Applied Acoustics 70 (4) (2009) 563–578.

[31] L. Maxit, V. Denis, Prediction of flow induced sound and vibration of periodically stiffened plates, J. Acoust. Soc. Am. 133 (1) (2013) 146–160.

[32] J. Kha, M. Karimi, L. Maxit, A. Skvortsov, R. Kirby, An analytical approach for modelling the vibroacoustic behaviour of a heavy fluid-loaded plate near a free surface, Journal of Sound and Vibration 538 (2022) 117206.

[33] E. G. Williams, Fourier acoustics: sound radiation and nearfield acoustical holography, Academic press, London, UK, 1999.

[34] V. V. Krylov, New type of vibration dampers utilising the effect of acoustic'black holes', Acta Acustica united with Acustica 90 (5) (2004) 830–837.

[35] D. J. Mead, Plates with regular stiffening in acoustic media: vibration and radiation, The Journal of the Acoustical Society of America 88 (1) (1990) 391–401.

[36] C. Claeys, E. Deckers, B. Pluymers, W. Desmet, A lightweight vibro-acoustic metamaterial demonstrator: Numerical and experimental investigation, Mechanical systems and signal processing 70 (2016) 853–880.

[37] C. Kittel, P. McEuen, Introduction to solid state physics, John Wiley & Sons, 2018.

[38] J. Deng, N. Gao, X. Chen, Ultrawide attenuation bands in gradient metabeams with acoustic black hole pillars, Thin-Walled Structures 184 (2023) 110459.

Declaration of interests

☒The authors declare that they have no known competing financial interests or personal relationships that could have appeared to influence the work reported in this paper.

☐The authors declare the following financial interests/personal relationships which may be considered as potential competing interests: